Journal of Colloid and Interface Science 634 (2023) 336–345

Contents lists available at ScienceDirect

Journal of Colloid and Interface Science

journal homepage: www.elsevier.com/locate/jcis

Corrosion inhibitor distribution on abrasive-blasted steels

A. Krautsieder [a,c], N. Sharifi [b,c], D.C. Madden [b,c], J. Sonke [d], A.F. Routh [a,c], S.M. Clarke [b,c,*]

[a] Department of Chemical Engineering and Biotechnology, University of Cambridge, CB3 0AS Cambridge, UK
[b] Department of Chemistry, University of Cambridge, CB2 1EW Cambridge, UK
[c] Institute of Energy and Environmental Flows, University of Cambridge, CB3 0EZ Cambridge, UK
[d] Shell Global Solutions P. V., 1031 HW Amsterdam, The Netherlands

GRAPHICAL ABSTRACT

Hypothesis: Preferntial adsorption of BTAH on substrates present on abarasive blasted steel

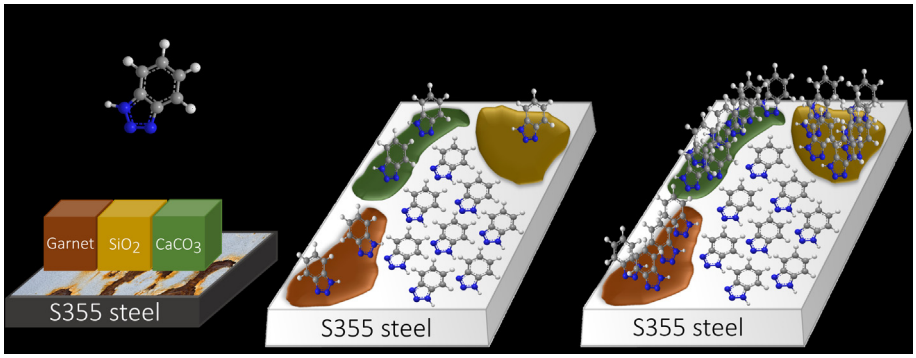

ARTICLE INFO

Article history:
Received 2 August 2022
Revised 24 October 2022
Accepted 2 December 2022
Available online 9 December 2022

Keywords:
Adsorption
Corrosion inhibition
Abrasive blasting
Steel maintenance

ABSTRACT

Hypothesis: Abrasive-blasted steel surfaces exhibit a complex, multi-substrate environment. Adsorption to contaminant substrates can reduce the amount of available corrosion inhibitor and decrease its efficiency. Knowledge of where inhibitors preferentially adsorb is required.
Experiments: The quantitative extent and strength of adsorption of the representative corrosion inhibitor benzotriazole (BTAH) from toluene to particular substrates is given, including corrections for solution self-association, and complemented by X-ray photoelectron spectroscopy (XPS), sum-frequency generation spectroscopy (SFG), and quartz crystal microbalance (QCM) measurements.
Findings: All substrates show adsorbed BTAH layers. Based on the adsorption strength, preferential adsorption is found to be in the order steel > iron oxide > calcium carbonate and garnet > silica – this is relevant when there is limited BTAH. However, with ample BTAH, the amounts adsorbed in the plateau regions of the isotherm are more relevant and the order is calcium carbonate and silica > iron oxide > garnet > steel. Although the contaminant substrates deplete the BTAH concentration, the steel should still have a complete monolayer of BTAH inhibitor. This work is part of a larger initiative developing novel methods of corrosion inhibitor delivery via the blasting process, to prevent corrosion between blasting and repainting.

1. Introduction

It has been recently demonstrated that 'cleaning' metal structures with abrasive blasting can lead to the presence of a number of inorganic solids, in addition to the metal/metal oxide substrate

* Corresponding author at: Department of Chemistry, Cambridge University, Lensfield Road, Cambridge CB2 1EW, UK.
E-mail address: sc10015@cam.ac.uk (S.M. Clarke).

https://doi.org/10.1016/j.jcis.2022.12.003
0021-9797/

[1]. These solids are embedded in, or deposited on, the metal surface and may be the major components of the abrasive, as well as other minor components. Interestingly, some minor components of the abrasive medium may be selectively enhanced at the surface depending on the way they adhere during blasting.

In this paper, we focus on these 'impurity' substrates, demonstrated to be present when steel infrastructure, such as offshore structures, are blasted as part of the cleaning/repair process. Current approaches still lead to corrosion and the need for expensive maintenance, including repeated cleaning and repainting. This work is part of a larger initiative to develop a novel method to deliver corrosion inhibitors as part of the blasting process, to address the issue of corrosion beginning in the period between blasting and repainting [2]. Whatever the delivery mechanism, many commercial inhibitors could be used. This work aims to illustrate the key issue of inhibitor distribution for a representative example.

This study builds on previous work concerning the adsorption of paint-relevant species [1]. Here, the adsorption of a representative corrosion inhibitor, 1*H*-benzotriazole (BTAH), is considered, adsorbed from non-aqueous solution to typical substrates one might find in an abrasive-blasted system (S355 steel, iron oxide, garnet, calcium carbonate and silica). Experimental data for the adsorption of BTAH on these different substrates are presented and compared.

It is common to use various surface-active agents as corrosion inhibitors in protective coatings, to minimize steel corrosion during paint drying, water ingress, and coating failure. These inhibitors are believed to function by adsorbing onto the metal surface. There are reports that in aqueous media these may work by forming a well-packed molecular 'barrier' layer at the metal surface [3-5]. However, recent neutron reflectivity studies have demonstrated that systems with an essentially perfect close-packed molecular layer still can corrode very quickly. By contrast, other much less perfect organic layers (less closely packed, with higher degrees of conformational disorder and higher solvent content) can inhibit corrosion effectively [6,7]. The difference in corrosion rate is attributed to the chemistry of the additive functional group, rather than any restricted layer permeability. These findings are also supported by measurements of the permeabilities of relatively thick paint films [8]. It may be inferred that a layer of molecular dimensions gives a rather limited barrier to migration.

A quantitative understanding of adsorption on different surfaces is essential to correctly predict how much additive is adsorbed on the surface of interest and how much is adsorbed on other accessible materials. It is to be expected that there will be some preferential adsorption, and if the metals to be protected cannot compete effectively, the other substrates can act as a sink, removing the inhibitor from the system and leaving the metals exposed. For example, if one wishes to protect a steel surface in the presence of a significant amount of embedded garnet: if the inhibitor preferentially adsorbs on the garnet, less inhibitor will be available to protect the steel. It has been reported that impurities acting as competing surfaces can indeed reduce the performance of corrosion inhibitors on steel, highlighting the need for detailed analysis of corrosion inhibitor behaviour in complex industrial settings [9]. This predicament could be dealt with by adding more inhibitor to the system to ensure there is enough to cover the competing surfaces and the steel, but that may be an unnecessary expense if the steel is the dominant site of adsorption.

BTAH is reported to act as a corrosion inhibitor on various metallic substrates, such as iron, copper and aluminium [10-13]. On copper, the molecules are reported to be adsorbed in an essentially upright orientation, with the ring perpendicular to the surface and the nitrogen atoms pointing towards the surface. Some reports state that BTAH molecules deprotonate and form stable complexes with copper surface atoms and adatoms, building up chains across the surface [13-15]. Anti-corrosive properties of BTAH have also been reported for aluminium, iron and steel surfaces, but with decreased efficiency compared to copper [10,16]. In aqueous systems, BTAH has been found to interact with iron atoms at iron or steel surfaces by deprotonation of the inhibitor molecule [17-19]. This interaction appears to be similar to, but slightly weaker than, the interaction between BTAH and copper, with the triazole moiety oriented towards the metal surface [18]. The adsorption of BTAH from aqueous solutions is pH dependent: complex formation with iron surface atoms has been reported to occur in neutral and slightly basic conditions [17-21], whereas under acidic conditions, the BTAH is said to form a molecular layer [19]. The reports also suggest that the strength of BTAH adsorption varies depending on the pH; on iron and steel, values consistent with both physisorption and chemisorption have been reported [17-19,22]. Literature illustrating steel corrosion with and without BTAH is given by Sabet Bokati *et al.* [10,16] and Section S1 in the Supporting Information shows similar data collected by the present authors.

Many surface-active additives in commercial formulations are amphiphilic, with polar head groups and non-polar alkyl tails. In non-aqueous solvents, the polar head groups are not expected to be well dissolved and may self-associate. Therefore, not all of the additive in solution will be present in the monomer form: a large fraction, indeed the majority, may be present as associates. The behaviour (such as adsorption) of these solutions is controlled by the monomer chemical potential, not the total amount present. As the total amount of additive increases, the amount of monomer may not change substantially, if there is significant association occurring. Therefore, the amount adsorbed will not change and will appear to have reached an adsorption plateau. This behaviour is similar to that of micellizing surfactants in water above the critical micelle concentration.

Self-association in aprotic solvents has been reported for many nitrogen-containing bases, leading to multimers of various orders depending on the molecular species and solvent [23]. Determining association constants for nitrogen-containing bases is challenging and depends on the experimental conditions and assumptions [24]. In this work, literature values of the association constants have been used to estimate the magnitude of this effect and hence its role when quantifying the extent of adsorption; full details are given in section S2 in the Supporting Information. In brief, knowledge of the equilibrium constants allows the extent of association and monomer concentration to be determined for any total BTAH concentration. This monomer concentration is then used to assess the adsorption behaviour. The solution association constants used here were taken from the paper by White *et al.*, which considered the association of BTAH in benzene [25]. These constants are expected to be a reasonably good approximation to those in toluene. One might consider toluene slightly more alkane-like than benzene, which usually leads to more self-association, so these calculations are likely to be a slight underestimate. Section S2 in the Supporting Information outlines the mathematical expressions required; Matlab was used to calculate the monomer concentrations.

2. Experimental section

Chemicals and reagents. 1*H*-benzotriazole (BTAH, 99 %) was purchased from Sigma-Aldrich, and toluene (99.85 %, extra dry) was supplied by Acros Organics. The adsorbent materials, iron oxide (Fe_2O_3, haematite; BET surface area 6.05 ± 0.01 $m^2\ g^{-1}$) and fumed silica (BET surface area 187.7 ± 1.6 $m^2\ g^{-1}$), were purchased from Sigma Aldrich. Minerals Technologies supplied precipitated calcium carbonate (BET surface area 16.75 ± 0.04 $m^2\ g^{-1}$),

and S355 steel powder was supplied by Sandvik Osprey (BET surface area 0.30 ± 0.01 $m^2\ g^{-1}$). All materials were used as received. 80 Mesh (177 μm) almandine garnet powder was purchased from GMA Garnet and was milled to a reduced size of below 10 μm. This material was treated with acid to remove a calcium carbonate impurity, as described elsewhere [1]. The BET surface area of the acid-treated garnet powder, as used in the adsorption experiments, was determined as 6.59 ± 0.05 $m^2\ g^{-1}$.

Adsorption determined by solution depletion. The adsorption of BTAH on these selected adsorbent materials at room temperature and standard pressure was characterized by the solution depletion method. 10 mL of known concentrations of BTAH in toluene was added to 2 g of iron oxide powder, 2 g of precipitated calcium carbonate, 0.35 g of fumed silica, 2 g of garnet powder, or 10 g of S355 steel powder, respectively, in 22 mL glass vials. The mixtures were tumbled for 4 h. This time was optimized based on a time-dependent measurement to ensure complete equilibration of the system and minimize potential solvent evaporation. After centrifugation of the mixture for 30 min at 10,000 rpm, the clear supernatant was retrieved, and the concentration of BTAH was determined by ultraviolet–visible spectroscopy relative to calibration measurements. The amount of BTAH adsorbed was determined by the difference of concentrations measured before and after equilibration.

Ultraviolet–visible spectroscopy (UV–vis). The concentrations of BTAH in toluene were determined at a wavelength of 290 nm using a Cary 60 UV–visible Spectrophotometer, Agilent Technologies, and Hellma Suprasil quartz absorption cuvettes of 3 mL volume and 10 mm pathlength.

QCM desorption measurement. In this work, a Biolin Qsense at the Department of Nanotechnology, University of Cambridge was used. Quartz QCM chips coated with iron oxide (Fe_2O_3, haematite) were obtained from Biolin and initially exposed to pure toluene, establishing a stable baseline. BTAH solutions were then exposed to the substrate, and the shift of frequency and dissipation noted. It is expected that the adsorbed layers will be fairly rigid; hence the frequency shift, indicative of the adsorbed monolayer mass loading, can be assessed with the Sauerbrey equation. The observed dissipation supports such an interpretation, with changes in dissipation, ΔD, remaining below 0.5 ppm (Section S3 in the Supporting Information). The adsorption isotherm was assessed by following the frequency shift with a series of solutions of increasing concentration. Finally, flushing with a pure solvent was used to assess the desorption and any reversibility of the adsorption process.

3. Results and discussion

Experimentally determined adsorption isotherms of 1*H*-benzotriazole (BTAH) in toluene on iron oxide, calcium carbonate, silica, and garnet by the solution depletion method are given in Fig. 1. The data are presented in terms of the monomer concentration of BTAH. With all substrates, there is a pronounced rise in adsorption with increasing concentration in solution. However, the rise in adsorption slows at higher concentrations, and a plateau in adsorption is generally evident, although this is discussed in more detail for each system below. The specific adsorption values plotted in Fig. 1 were calculated using the substrate-specific surface areas, measured independently by BET analysis. However, it is important to note that measurements of specific surface areas have significant uncertainties.

Fig. 2 shows the adsorption data of BTAH from toluene on iron oxide and calcium carbonate at 20 °C. The adsorbed amount is plotted as a function of the total BTAH present in the solution (squares) and as a function of the monomer concentration (circles). To give

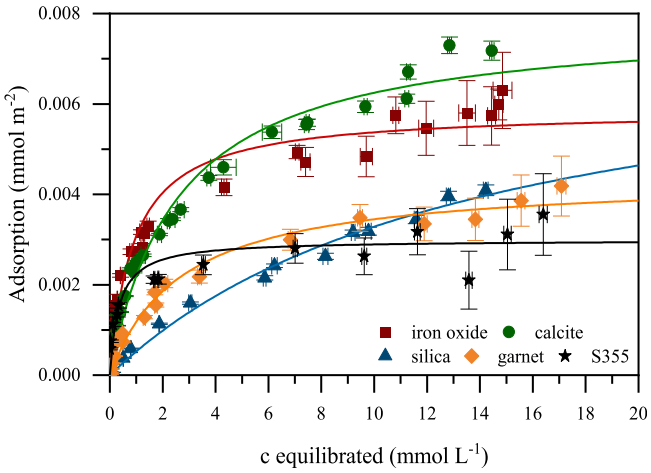

Fig. 1. Adsorption isotherms of 1H-benzotriazole (BTAH) in toluene on iron oxide, calcium carbonate, silica, garnet, and S355 steel surfaces at 20 °C with respective Langmuir isotherm fits; concentrations are monomer concentrations.

an estimate of the role of self-association, for a 10 mM total concentration, 22 % of the total amount of BTAH is associated. The data plotted in terms of the monomer concentration have the same form as plotted in terms of the total BTAH concentration, but now the features are moved to lower concentration, and any 'plateau' is less pronounced. However, it is important to note that the appearance of the plots at the lowest concentrations is not significantly altered.

Fig. 3 presents similar isotherm data for BTAH on silica, acid-washed garnet and S355 steel. Many of the features identified above for BTAH on iron oxide and calcium carbonate are again seen, for example a reasonably sharp rise with concentration to a modest plateau. In some cases, after correction of the horizontal axis to monomer concentration, there is an apparent further increase in adsorption which appears to suggest a divergence somewhere between 20 and 30 mmol L^{-1}, as discussed further below.

The key features of the isotherms are a) the 'plateau' value, a measure of the substrate area per adsorbed molecule and b) the initial gradient, which is directly related to the free energy of adsorption and is a measure of the 'strength of adsorption'. The change from plotting the total concentration to plotting the monomer concentration moves the data to the left, parallel to the concentration axis. Hence, the magnitude of the adsorption plateau is not generally affected. The initial gradient of the isotherm could be changed by any low-concentration translation on the concentration axis. However, at the very low concentrations, where we observe this rapid rise in adsorption, our calculations and Figs. 2 and 3 indicate there is expected to be rather little self-association, and the initial slopes of the isotherms remain essentially unchanged.

All the data in Figs. 2 and 3 have been fitted to a Langmuir isotherm model (as outlined in section S4 in the Supporting Information) as a function of monomer concentration. According to this model, K_L is the adsorption equilibrium constant, and Γ_∞ is the plateau adsorption value.

The experimental data were also fitted with the BET isotherm (described in detail in section S4 in the Supporting Information). This model has parameters which can be stated as K_1: the equilibrium constant for the adsorption of the BTAH directly to the substrates, K_n: the equilibrium constant for adsorption of BTAH onto already adsorbed BTAH, and Γ_{inf}: a parameter characterizing the monolayer coverage [26,27]. The extracted fit parameters for all systems are summarised in Table 1.

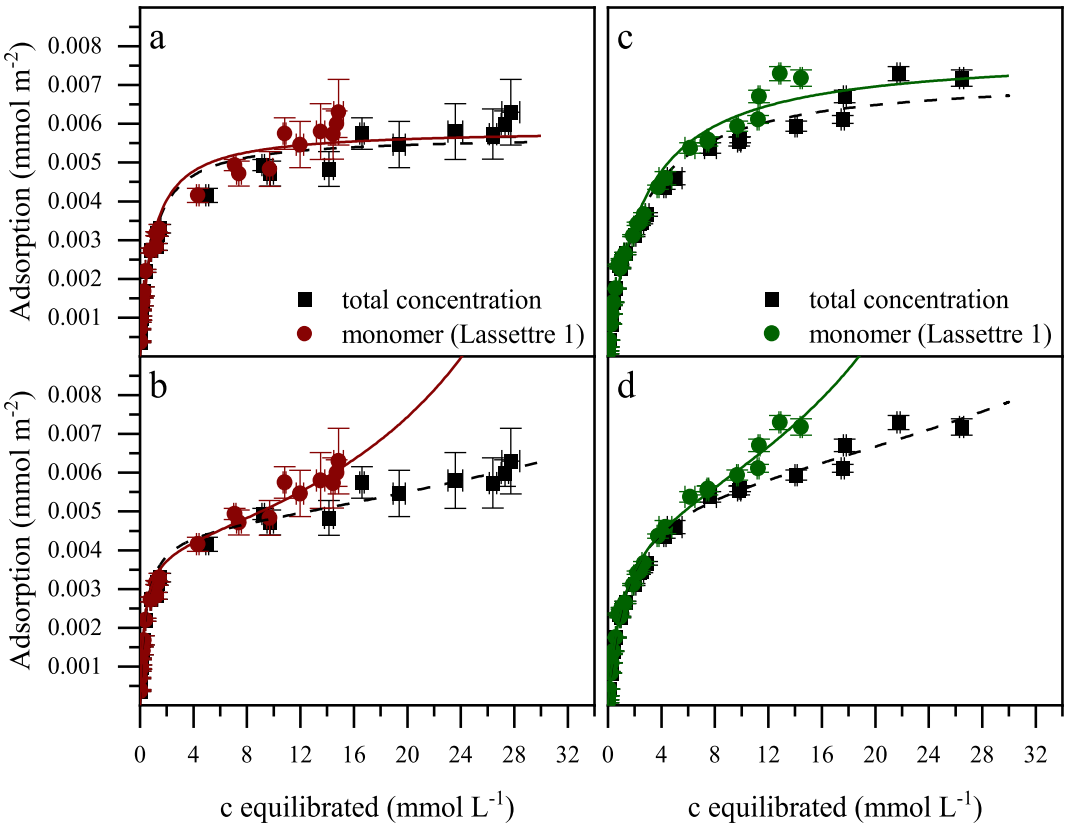

Fig. 2. BTAH adsorption from toluene on iron oxide (a: Langmuir model fit, b: BET model fit) and calcium carbonate (c: Langmuir model fit, d: BET model fit) at 20 °C. The data are presented as total concentration (squares) and monomer concentration (circles).

The BET model captures several features of the experimental data not captured by the Langmuir model. In particular, the divergence of the adsorption at high concentration can be interpreted as the approach to the miscibility limit when the BTAH becomes insoluble: It is possible to demonstrate that the equilibrium constant K_n is given by $1/C_{sat}$, where C_{sat} is the saturation concentration of the BTAH/toluene solution. The solubility limit has been determined experimentally as 31.7 ± 1.6 mmol L^{-1} (stated as the total concentration, not the monomer concentration; experimental details are given in section S5 in the Supporting Information), which leads to a K_n value of 31.5 ± 1.6 M^{-1}. The solubility limit shows reasonable agreement with the concentration at which the adsorption is observed to diverge, and the K_n value obtained from the solubility limit is comparable to those found from the BET fits to the isotherm data (given in Table 1), supporting the interpretation that the apparent divergence in adsorption is due to the BTAH concentration approaching saturation.

3.1. Areas per molecule in the plateau region

The plateau values of the isotherms in Figs. 2 and 3 can be used to estimate the effective surface area per molecule of BTAH, A_L. Geometric estimates of the molecular size (described in detail in section S6 in the Supporting Information) have been made to interpret the magnitude of these A_L values; the molecular area of the BTAH ranges from 20 $Å^2$, the case with the plane of the aromatic rings perpendicular to the surface, to 52 $Å^2$, when the rings are parallel to the surface, as illustrated in Fig. 4.

The areas per molecule, A_L, of BTAH on iron oxide, calcium carbonate, and silica extracted from the isotherm data are well below 52 $Å^2$ and not dissimilar to 20 $Å^2$. Hence, these area-*per*-molecule values indicate an essentially upright BTAH molecule. This orientation is perhaps not unexpected, given the likelihood of a particularly strong interaction of the nitrogens with the substrates, and is in good agreement with the literature concerning BTAH on copper [13,31-33]. In the cases of garnet and S355 steel, the higher areas per molecule suggest a more tilted orientation of BTAH on the surface. This is consistent with findings for butyl imidazole adsorption on steel, where the azole ring has been found to be oriented in plane with the substrate surface, or slightly tilted. Butyl imidazole molecules were less closely packed on steel compared to adsorption at a copper surface, where the azole ring was oriented in an upright configuration, similar to the behaviour of BTAH on copper [34].

The BET fitting also provides the areas per BTAH molecule in the first monolayer, A_{BET}; these are given in Table 1. These are somewhat larger than the values found using the Langmuir model (A_L), suggesting that the molecules are not as tightly packed on the surface as previously implied and may be more significantly inclined. The larger area per molecule is consistent with the shape of the BET fits, in which the 'plateau' regions of the isotherms are not particularly flat/horizontal, effectively indicating that adsorption to subsequent layers becomes significant before the monolayer is complete.

3.2. Substrate sites

It is important to consider if the maximum monolayer density is due to the packing size of the BTAH molecule or arises from the 'reaction' of the BTAH with well-defined surface sites. Chemisorption tends to be of this latter type, due to the strong energy benefit of substrate-molecule binding. It has been proposed that BTAH is chemisorbed onto copper, while both chemisorption and physisorp-

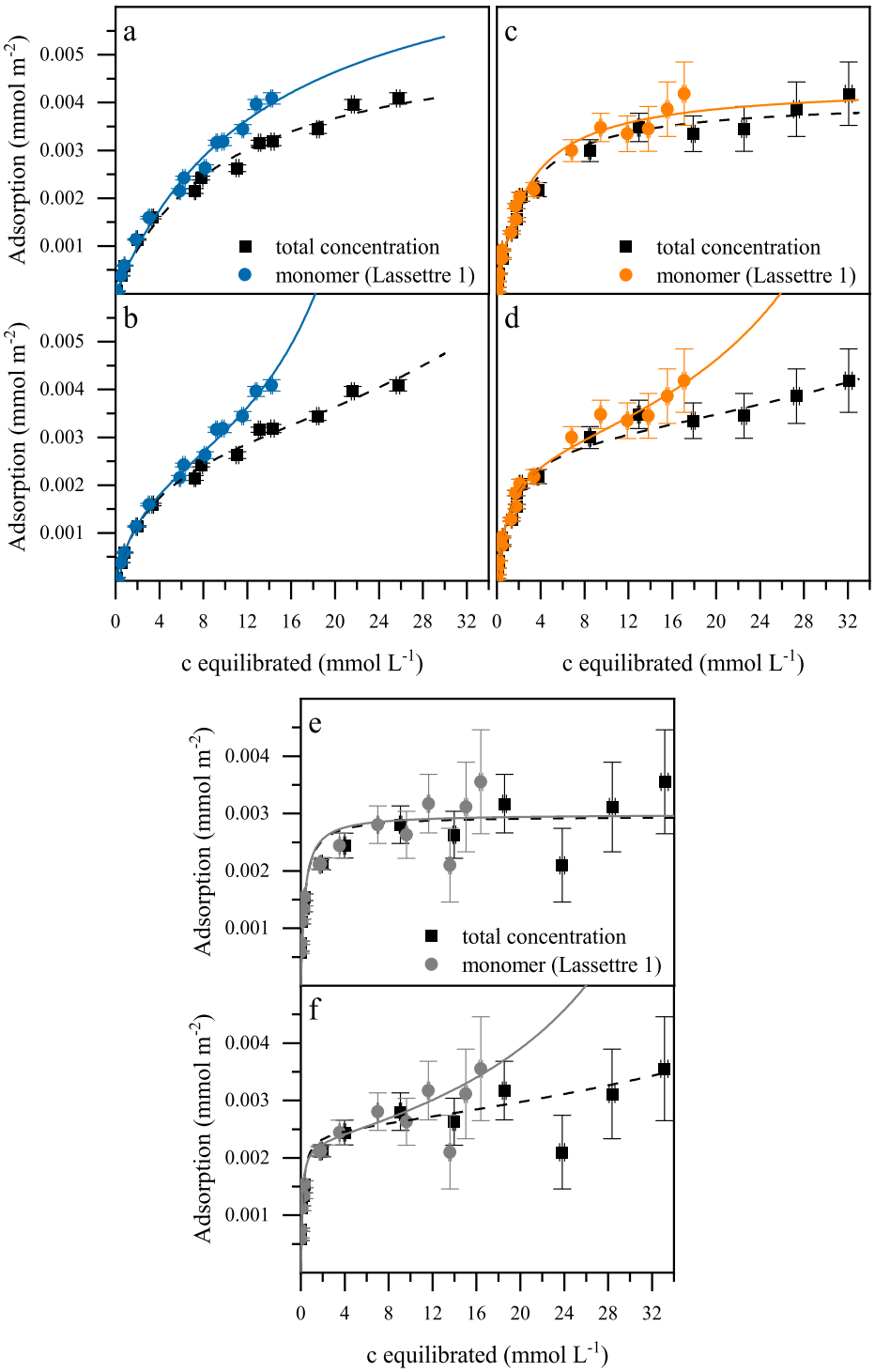

Fig. 3. BTAH adsorption from toluene on silica (a: Langmuir model fit, b: BET model fit), garnet (c: Langmuir model fit, d: BET model fit) and S355 steel (e: Langmuir model fit, f: BET model fit) at 20 °C. The data are presented as total concentration (squares) and monomer concentration (circles).

tion have been reported on other surfaces, such as mild steel and aluminium alloys [10].

The surface site density has been estimated for each of the substrates, to compare with the isotherm data: Surface hydroxyl groups are often reported to play a predominant role in the surface chemistry of iron oxides [35]. The average hydroxyl group density at the surface of haematite, a typical iron oxide, is reported to be 4.4 sites nm^{-2}, equivalent to 22.7 $Å^2$ per site, although a range of values have been found, dependent on the experimental method [28]. The area per active surface site for calcium carbonate is taken as 20.4 $Å^2$ [29], and that for silica is 21.7 $Å^2$ [30]. The acid-treated garnet surface has previously been estimated to have 95.2 $Å^2$ per site by surface titration [1]. The area per active site on the S355 steel surface was estimated, by determining the percentages of crystallographic mineral phases present (using backscattered electron diffraction data from a polished surface) and attributing the hydroxyl group densities reported for various well-characterized

Table 1
Summary of BTAH adsorption isotherm values of monomer concentration data.

Adsorbent	K_L (M^{-1}) x 10^3	Monolayer adsorption Γ_∞(mmol m^{-2})	R^2	Area per molecule A_L (Å^2)	Area per surface site (Å^2) (inferred from literature values)
Iron oxide	1.1 ± 0.1	0.0059 ± 0.0009	0.947	28 ± 4	22.7[28]
Calcium carbonate	0.39 ± 0.03	0.0079 ± 0.0005	0.979	21 ± 1	20.4[29]
Silica	0.07 ± 0.01	0.0079 ± 0.0004	0.991	21 ± 1	21.7[30]
Garnet	0.36 ± 0.05	0.0044 ± 0.0004	0.981	37 ± 4	95.2[1]
S355 steel	3.0 ± 0.3	0.0030 ± 0.0005	0.838	56 ± 9	19.1[1]
	K_1 (M^{-1}) x 10^3	K_n (M^{-1}) x 10^3	Monolayer adsorption Γ_∞(mmol m^{-2})	R^2	Area per molecule A_{BET} (Å^2)
Iron oxide	3.2 ± 0.8	0.023 ± 0.008	0.004 ± 0.001	0.997	40 ± 15
Calcium carbonate	0.90 ± 0.06	0.024 ± 0.002	0.0050 ± 0.0005	0.996	33 ± 1
Silica	0.38 ± 0.03	0.034 ± 0.004	0.0024 ± 0.0003	0.983	68 ± 8
Garnet	0.9 ± 0.1	0.023 ± 0.004	0.0027 ± 0.0005	0.992	62 ± 12
S355 steel	8.8 ± 1.0	0.021 ± 0.002	0.0023 ± 0.0003	0.994	73 ± 18

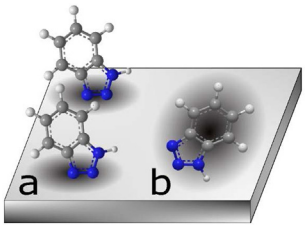

Fig. 4. Possible configurations of a BTAH molecule on a surface; a. with the plane of aromatic rings perpendicular to the surface (giving an estimated area per molecule of 20 Å^2); b. with the plane of aromatic rings parallel to the surface (52 Å^2 per molecule).

iron oxides, as 19.1 Å^2 (5.3 sites nm^{-2}) [1]. These site-dependent areas are summarised in Table 1.

For iron oxide, calcium carbonate and silica, the areas per surface site correspond well with the areas per BTAH molecule, evaluated using the Langmuir model, suggesting that approximately every active site is occupied by one molecule. The smaller area per molecule compared to the area per site for the garnet powder could be interpreted as the interaction of multiple BTAH molecules with each active surface site, although this finding could also be caused by underestimating the number of sites for the rather inhomogeneous garnet material. Popova *et al.* reported that BTAH adsorbs on Al_2O_3 surfaces via hydrogen bonds to Al-OH surface groups. They postulated that the deprotonation of BTAH during this process causes the formation of additional adjacent Al-OH groups [36]. Neighbouring Al-OH groups could take up the BTAH proton, forming Al-OH$^+$ which in turn could separate into Al^{3+} and H_2O. If H_2O desorbs from the surface in this way, a small amount of water will be present (even though the solvent is non-polar), which is able to further react with the surface. A mechanism such as this would lead to more available reaction sites and thereby effectively decrease the area per site. In the case of S355 steel, the packing of substrate sites is too close for this relatively large molecular species to fit on every site. The area per BTAH molecule obtained from the Langmuir fit is significantly larger for S355 than the other substrates considered here, consistent with the molecules adopting a relatively flat conformation, or, if a direct reaction is the dominant interaction mechanism, the molecules adsorbing on every third site.

3.3. Comparison of adsorption plateaus

When fitted with a Langmuir adsorption model, the plateau value for the adsorption of BTAH on S355 steel is approximately half the plateau value for the data on iron oxide (haematite) powder. It might initially be expected that the steel has a surface of iron oxide, and there should be a better agreement. However, the mineral composition of the steel surface layer can be complex and changes depending upon the chemical and thermal history of the samples. In a previous report it has been suggested that for the steel used in this study, the predominant iron oxide species is magnetite (47.7 %) rather than haematite (15.5 %), and the average hydroxyl group densities on magnetite (5.2 nm^{-2}) and haematite (4.4 nm^{-2}) are different [1]. Therefore, the difference in monolayer adsorption behaviour is likely to be due to these substrate differences.

The determination of the amounts of BTAH adsorbed on the different substrates (particularly steel) requires a detailed, case-by-case calculation using the determined adsorption parameters with estimates of the amounts of each substrate present. However, a simple overview based on the relative adsorption strengths and amounts might be considered as follows:

At high concentrations of BTAH the plateau values (Table 1) determined by fitting the Langmuir model to the data are in the order calcium carbonate ~ silica > iron oxide > garnet > S355 steel. The amount of adsorbed BTAH in the monolayer found from BET fits (Table 1) shows a slight variation in the order: calcium carbonate > iron oxide > garnet > silica > S355 steel. This finding implies that a significant amount of BTAH can be adsorbed on the mineral substrates, which could lead to losses from the BTAH reservoir and leave less BTAH available for adsorption on the steel.

However, as these high degrees of adsorption are only achieved for high solution concentrations of BTAH, it can be assumed that, despite the adsorption on the other substrates, the remaining BTAH concentration should still be sufficient for complete coverage of the steel surface, and the corrosion inhibition efficiency should not be affected. But, for limited concentrations of BTAH in solution, the mechanism of preferential adsorption is governed by the strength of adsorption of the BTAH molecules on the different substrates. Therefore, adsorption energies were determined and compared.

3.4. Thermodynamic energies of adsorption

The changes in the Gibbs free energy of adsorption, ΔG_{ads}, can be calculated from the evaluated Langmuir equilibrium constants, K_L, or BET first-layer equilibrium constants, K_1, using Equation **(1)** [37]. R is the gas constant, whose value is 8.314 J mol^{-1} K^{-1}, T the absolute temperature in Kelvin, and K a general thermodynamic equilibrium constant of adsorption (substituted by K_L or K_1).

$$\Delta G_{ads} = -RTlnK \quad (1)$$

The respective changes in the free energies of adsorption for the formation of a monolayer and BET first layer, ΔG_L and ΔG_1, are given in Table 2 and are used to compare the 'strength' of adsorption on different substrates.

As noted in section S7 in the Supporting Information, the initial gradient of an adsorption isotherm is directly related to the equilibrium constant for adsorption: Evaluation of the initial gradients for the data in Fig. 1 produced equilibrium constants in very good agreement with the values from the Langmuir fitting. Therefore, only the results from the Langmuir and BET fits are discussed further.

Negative values for the changes in free energy reflect that the adsorption of BTAH from toluene is energetically favorable for all tested substrates; as expected, the adsorption is spontaneous. The ΔG_{ads} values calculated from Langmuir and BET equilibrium constants correlate well, showing the same trend in the strength of adsorption of BTAH from toluene onto the tested substrates. The sequence of adsorption strength goes as S355 steel > iron oxide > calcium carbonate ~ garnet > silica.

The determined values are in accordance with previously reported data for BTAH adsorption from aqueous solutions. Yang *et al.* reported adsorption free energies around 35 kJ mol^{-1} for BTAH on copper from sodium chloride solution [33]. Bokati *et al.* analyzed the adsorption of BTAH from artificial seawater onto mild steel and an aluminium alloy by weight loss measurements (indicative of the corrosion rate); they stated ΔG_{ads} as –22.69 kJ mol^{-1} for mild steel and –23.97 kJ mol^{-1} for an aluminium alloy [10]. Similar values were found for the adsorption of BTAH from various aqueous solutions onto steel surfaces [22]. However, Walczak *et al.* recently pointed out that estimating the standard Gibbs free energy of adsorption from inhibition efficiency (by inferring the fractional surface coverage), rather than from adsorption directly, may not give values that are particularly reliable, because the actual nature of adsorption and amount adsorbed are unknown [38].

DFT calculations of the gas-phase adsorption of BTAH onto the Fe{1 1 0} surface reported that the BTAH molecule lies flat on the surface, with an adsorption energy of −130 kJ mol^{-1} [39]. Considering that substrates are typically not ideal, with defects and non-equivalent adsorption sites, and the competition from the solvent molecules for available adsorption sites, it can be assumed that the energy changes and preferred molecule orientations in such systems will be affected.

It is noted that, although the differences in ΔG_{ads} on the different substrates considered here appear to be small, the amount of BTAH adsorbed onto contaminant substrates on steel is controlled by the corresponding equilibrium constants (Equation **(1)**), as presented in Table 1. Therefore, even small differences in free energy can have a significant effect on the adsorbed amount of BTAH for a specific solution concentration. Based on the results obtained here, preferential adsorption of BTAH onto S355 steel and iron oxide over the other mineral impurities can be assumed. However, adsorption losses of any corrosion inhibitor will occur and have to be accounted for, particularly if there is a lot of impurity present; this again highlights the importance of analysing the adsorption onto the contaminant species that are present in complex industrial settings.

Table 2
Gibbs free energy of adsorption of BTAH onto various substrates from toluene at 20 °C, calculated using the adsorption equilibrium constants of the Langmuir (K_L) and BET (K_1) isotherm fits.

Adsorbent	ΔG_L (kJ mol^{-1})	ΔG_1 (kJ mol^{-1})
Iron oxide	−17.1 ± 0.2	−19.7 ± 0.6
Calcium carbonate	−14.5 ± 0.2	−16.6 ± 0.2
Silica	−10.4 ± 0.3	−14.5 ± 0.2
Garnet	−14.4 ± 0.3	−16.6 ± 0.3
S355 steel	−19.5 ± 0.2	−22.1 ± 0.3

3.5. XPS

XPS data on the adsorption of BTAH to S355 steel substrates are given in section S8 in the Supporting Information. This experiment was intended to confirm the presence of BTAH and indicate the nature of its interaction with the substrate, particularly the role of the nitrogen atoms, which may be expected to electron donate to the surface. The appearance of a N1s peak after treatment of steel substrates with solutions of BTAH in toluene confirmed the presence of the inhibitor on the surface. However, no significant changes in the shapes of the N1s and C1s peaks from those seen for unadsorbed BTAH could be observed. A slight change in the peak position could not be futher interpreted, as it could arise from the calibration method used. The reason for this could lie in a small shift of the C1s peak in the pure BTAH spectrum due to an overlap of the BTAH carbon signal and the adventitious carbon peak that is used for calibration of the steel samples. Hence, we may conclude that the local electronic environments of these atoms are not significantly perturbed on adsorption, suggesting a weak adsorption (possibly physisorption).

It is noted that the sample preparation is crucial: These samples are prepared by dipping a steel coupon in BTAH solution, removing it and drying under a nitrogen stream, before the XPS measurement. Although great care was taken to avoid small drops of bulk solution remaining on the substrate by tilting the coupon and running the nitrogen stream over the sample, even a small drop will evaporate and deposit a significant amount of BTAH, dwarfing the signal of interest from the first adsorbed molecular layer. However, previous DFT and experimental work investigating a single BTAH layer on copper has indicated that, even if the three nitrogen atoms are in distinct environments, they cannot be resolved in most XPS instruments [40].

3.6. Adsorption and desorption study with QCM

Fig. 5 presents the normalized change in frequency during the addition of increasing concentrations of BTAH in toluene to an iron oxide-coated QCM chip. The data show a series of step changes in

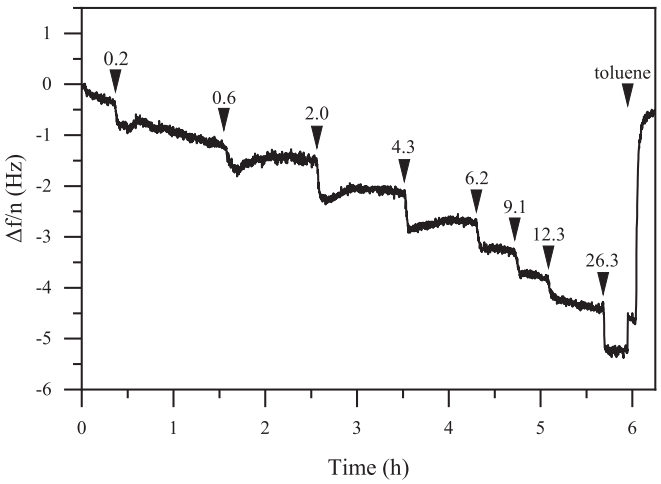

Fig. 5. Changes in frequency (at the 11th overtone) as a function of time, during the stepwise addition of different concentrations of BTAH in toluene to an iron oxide-coated QCM chip at 20 °C. Arrows indicate the times the concentrations were added, with numbers referring to the respective BTAH concentrations in mmol L^{-1}.

frequency with increasing concentrations, again indicating the adsorption of the BTAH. This shift is seen in several harmonics that all respond in a similar fashion. The adsorbed masses were deduced, and the resulting adsorption isotherm is compared to that obtained by depletion in Fig. 6. The error bars on the isotherm reflect the variation in repeats of the experiment, and also the variation when different overtones are used to extract the adsorbed amounts.

Fig. 6 indicates that the qualitative trends of the isotherms measured by the two methods (depletion and QCM) are very similar, with rises in adsorption that reach plateaus over the same concentration range. The QCM and solution-depletion adsorption data correlate well, but the absolute values of the initial adsorption gradient and plateau from the two methods differ somewhat. These discrepancies can be attributed to several issues: The exposed surface area of the iron oxide on the QCM chip cannot be measured and may not be equal to the geometric area; deposition of what is essentially a powder may mean that the actual surface area is somewhat greater. Similarly, as mentioned above, the specific surface areas of the powders used for solution depletion are difficult to determine experimentally.

An important aspect also evident in the QCM data (Fig. 5) is that, after exposing the QCM chip to highly concentrated BTAH solution and adsorbing a significant layer, the exposure of this adsorbed BTAH layer to pure toluene leads to a return of the frequency to that essentially corresponding to the bare substrate. Hence, we conclude that the adsorption of BTAH on iron oxide is reversible. There is a small variation between the initial and final values, which may suggest a small amount of irreversibly bound material, or a drift in the QCM baseline, which is very difficult to avoid over such a long period.

There seems to be some debate in the literature over whether BTAH is chemisorbed or physisorbed onto iron, iron oxide and other surfaces. Due to its capability to deprotonate and interact with substrates in a Lewis acid-base manner, most reports conclude that the adsorption of BTAH onto metal and metal oxide surfaces occurs by chemisorption [17,19-22,36]. In aqueous systems, this depends on the solution pH. Bokati *et al.* proposed that BTAH is physisorbed onto mild steel and aluminium alloy, due to the magnitude of the adsorption energies being too low to account for chemisorption [10]. Recently, Kokalj argued that the magnitude of ΔG_{ads} cannot be used as an indicative measure for physisorption or chemisorption [39]. They note that more detailed information on the state of adsorption from modelling and/or spectroscopic techniques is necessary to characterize the inhibitor-substrate interactions fully. The reversibility of the adsorption observed here suggests that the interaction between BTAH and the tested iron oxide substrate in a non-aqueous environment is dominated by physisorption.

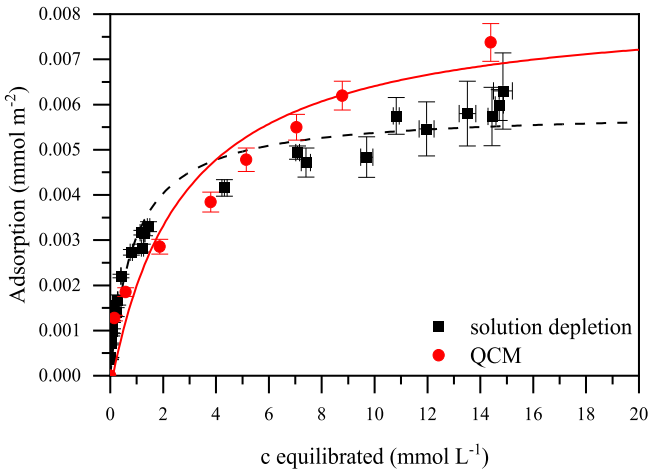

Fig. 6. BTAH adsorption from toluene on iron oxide powder measured by the solution depletion method (squares) and on an iron oxide layer deposited on a QCM chip (points), with respective Langmuir adsorption isotherm fits; concentrations have been converted to monomer concentrations.

3.7. SFG spectroscopy

SFG data were collected from the bare steel surface and with adsorbed BTAH (see section S9 in the Supporting Information); these were intended to confirm the adsorption of BTAH and ideally provide some indication of the molecular orientation, based on the presence/absence of BTAH vibrational modes with different polarisation combinations. In brief, the vibrational modes confirm the presence of BTAH. The presence, albeit weak, of the C—H stretching signals from the BTAH benzene ring in the SSP polarisation can be used to indicate that the adsorbed BTAH is not entirely flat on the surface of the substrate, and it is therefore inclined, in good agreement with the deductions from the adsorption isotherms. However, due to the high level of noise in the spectra, the magnitude of the inclination cannot be readily deduced.

4. Conclusions

The first quantitative assessment of the adsorption of 1*H*-benzotriazole (BTAH) from a non-aqueous solvent, toluene, onto several substrates relevant to abrasive cleaning of steel superstructures has been presented. In contrast to previous adsorption studies, we also consider the significance of self-association in the non-aqueous solution in the data interpretation. The data have been fitted to Langmuir and BET isotherm models with reasonable agreement. Although the proximity of the BTAH solubility limit leads us to conclude that the BET approach is preferred, the area per molecule determined from the Langmuir fits is generally smaller, which seems to correlate better with the experimental findings for the molecular orientation.

We find evidence of strong-but-reversible adsorption, leading to an essentially complete, well-packed monolayer at solution concentrations of 10 mM, when a Langmuir-type adsorption mechanism is considered. The BET model fits suggest the possibility of multilayer formation before completion of the monolayer, as well as an increased tendency for multilayer formation or sorption upon the approach of the solubility limit of BTAH in toluene.

The areas per molecule obtained from a Langmuir analysis suggest essentially upright orientations of the BTAH molecules on iron oxide, calcium carbonate and silica, and possibly tilted orientations on garnet and S355 steel. However, larger areas are deduced from the BET analysis, suggesting much flatter orientations. The SFG data suggest that there is some molecular inclination on the surface (rather than being completely flat), but the precise angle of inclination cannot be deduced.

The relative strengths of adsorption are found to follow the sequence S355 steel > iron oxide > calcium carbonate ~ garnet > silica. By contrast, the order in amounts adsorbed in the plateau region is calcium carbonate ~ silica > iron oxide > garnet > steel. For limited BTAH present (at low bulk concentrations), the order in terms of adsorption strength is most relevant and indicates that BTAH will preferentially bind to the steel and iron oxide surfaces, as desired. For higher concentrations of BTAH, we expect the other substrates to adsorb significant amounts; however, the steel/iron oxide should still have complete layers and effective corrosion inhibition.

Compared to the adsorption of BTAH in aqueous systems [10,15,16], this work builds a new understanding of BTAH in

non-aqueous solvents, which are commercially important in, for example, lubrication and oil-recovery, as well as extending previously published studies of paint-relevant additives on steel and garnet [1]. This work indicates that the adsorption of BTAH on other 'impurity' substrates is significant and inhibitor self-association, an effect which is often neglected, should be included.

The data presented enable calculations to estimate the complex implications for industrial applications due to the minerals present on abrasive-blasted surfaces. This approach should be applied (along with solution self-association studies) to other corrosion inhibitors, and under different conditions, to determine the extent of unfavourable preferential adsorption and the resulting negative effects on corrosion prevention. It could also be extended to consider novel solvent systems, such as supercritical CO_2, which is increasingly relevant due to the potential for corrosion in CCUS infrastructure.

CRediT authorship contribution statement

A. Krautsieder: Conceptualization, Investigation, Formal analysis, Visualization, Writing – original draft. **N. Sharifi:** Investigation, Formal analysis. **D.C. Madden:** Conceptualization, Supervision, Writing – review & editing. **J. Sonke:** Writing – review & editing. **A.F. Routh:** Resources, Supervision, Writing – review & editing, Funding acquisition. **S.M. Clarke:** Conceptualization, Resources, Supervision, Writing – original draft, Funding acquisition.

Data availability

Data will be made available on request.

Declaration of Competing Interest

The authors declare that they have no known competing financial interests or personal relationships that could have appeared to influence the work reported in this paper.

Acknowledgements

The authors thank Royal Dutch Shell for funding, particularly Hans Sonke, Tom Bos, and Sukanta Gosh, for their technical support. We thank Radomir Slavchov, QMUL for insightful discussions on solution association.

Appendix A. Supplementary material

Supplementary data to this article can be found online at https://doi.org/10.1016/j.jcis.2022.12.003.

References

[1] J. Poon, D.C. Madden, M.H. Wood, S.M. Clarke, Characterizing Surfaces of Garnet and Steel, and Adsorption of Organic Additives, Langmuir. 34 (2018) 7726–7737, https://doi.org/10.1021/acs.langmuir.8b01405.
[2] J. Poon, S.M. Collins, D.C. Madden, H. Sonke, S.M. Clarke, Characterization of Short Time Marine Corroded Surfaces, J. Electrochem. Soc. 166 (2019) C509–C519, https://doi.org/10.1149/2.0931914jes.
[3] Y. Zhu, M.L. Free, G. Yi, The effects of surfactant concentration, adsorption, aggregation, and solution conditions on steel corrosion inhibition and associated modeling in aqueous media, Corros. Sci. 102 (2016) 233–250, https://doi.org/10.1016/J.CORSCI.2015.10.012.
[4] B. Sanyal, Organic compounds as corrosion inhibitors in different environments — A review, Prog. Org. Coatings. 9 (1981) 165–236, https://doi.org/10.1016/0033-0655(81)80009-X.
[5] R. Lindsay, S.B. Lyon, Introduction to Control of Corrosion by Environmental Modification, in: B. Cottis, M. Graham, R. Lindsay, S. Lyon, T. Richardson, D. Scantlebury, H. Stott (Eds.), Shreir's Corros, Elsevier, 2010, pp. 2891–2899, https://doi.org/10.1016/B978-044452787-5.00159-1.
[6] M.H. Wood, T.J. Wood, R.J.L. Welbourn, J. Poon, D.C. Madden, S.M. Clarke, An X-ray and Neutron Reflectometry Study of Iron Corrosion in Seawater, Langmuir. 34 (2018) 5990–6002, https://doi.org/10.1021/acs.langmuir.8b00378.
[7] R.J.L. Welbourn, C.L. Truscott, M.W.A. Skoda, A. Zarbakhsh, S.M. Clarke, Corrosion and inhibition of copper in hydrocarbon solution on a molecular level investigated using neutron reflectometry and XPS, Corros. Sci. 115 (2017) 68–77, https://doi.org/10.1016/J.CORSCI.2016.11.010.
[8] G.W. Walter, A critical review of the protection of metals by paints, Corros. Sci. 26 (1986) 27–38, https://doi.org/10.1016/0010-938X(86)90120-4.
[9] B.P. Binks, P.D.I. Fletcher, I.E. Salama, D.I. Horsup, J.A. Moore, Quantitative prediction of the reduction of corrosion inhibitor effectiveness due to parasitic adsorption onto a competitor surface, Langmuir. 27 (2011) 469–473, https://doi.org/10.1021/la103570e.
[10] K. Sabet Bokati, C. Dehghanian, Adsorption behavior of 1H-benzotriazole corrosion inhibitor on aluminum alloy 1050, mild steel and copper in artificial seawater, J. Environ Chem. Eng. 6 (2018) 1613–1624, https://doi.org/10.1016/J.JECE.2018.02.015.
[11] T. Kosec, D.K. Merl, I. Milošev, Impedance and XPS study of benzotriazole films formed on copper, copper–zinc alloys and zinc in chloride solution, Corros. Sci. 50 (2008) 1987–1997, https://doi.org/10.1016/j.corsci.2008.04.016.
[12] M. Finšgar, I. Milošev, Inhibition of copper corrosion by 1,2,3-benzotriazole: A review, Corros. Sci. 52 (2010) 2737–2749, https://doi.org/10.1016/j.corsci.2010.05.002.
[13] C. Gattinoni, A. Michaelides, Understanding corrosion inhibition with van der Waals DFT methods: The case of benzotriazole, Faraday Discuss. 180 (2015) 439–458, https://doi.org/10.1039/C4FD00273C.
[14] I. Dugdale, J.B. Cotton, An electrochemical investigation on the prevention of staining of copper by benzotriazole, Corros. Sci. 3 (1963) 69–74, https://doi.org/10.1016/S0010-938X(63)80001-3.
[15] F. Grillo, D.W. Tee, S.M. Francis, H.A. Früchtl, N.V. Richardson, Passivation of copper: Benzotriazole films on Cu(111), J. Phys. Chem. C. 118 (2014) 8667–8675, https://doi.org/10.1021/jp411482e.
[16] K. Sabet Bokati, C. Dehghanian, S. Yari, Corrosion inhibition of copper, mild steel and galvanically coupled copper-mild steel in artificial sea water in presence of 1H-benzotriazole, sodium molybdate and sodium phosphate, Corros. Sci. 126 (2017) 272–285, https://doi.org/10.1016/j.corsci.2017.07.009.
[17] P.G. Cao, J.L. Yao, J.W. Zheng, R.A. Gu, Z.Q. Tian, Comparative study of inhibition effects of benzotriazole for metals in neutral solutions as observed with surface-enhanced Raman spectroscopy, Langmuir. 18 (2002) 100–104, https://doi.org/10.1021/LA010575P.
[18] J.L. Yao, B. Ren, Z.F. Huang, P.G. Cao, R.A. Gu, Z.Q. Tian, Extending surface Raman spectroscopy to transition metals for practical applications IV. A study on corrosion inhibition of benzotriazole on bare Fe electrodes, Electrochim. Acta. 48 (2003) 1263–1271, https://doi.org/10.1016/S0013-4686(02)00834-4.
[19] L.P. Kazanskii, I.A. Selyaninov, XPES of 1,2,3-benzotriazole nanolayers formed on iron surface, Prot. Met. Phys. Chem. Surfaces. 46 (2010) 797–804, https://doi.org/10.1134/S2070205110070117.
[20] M.M. Mennucci, E.P. Banczek, P.R.P. Rodrigues, I. Costa, Evaluation of benzotriazole as corrosion inhibitor for carbon steel in simulated pore solution, Cem. Concr. Compos. 31 (2009) 418–424, https://doi.org/10.1016/j.cemconcomp.2009.04.005.
[21] S.-J. Huo, J.-Y. Wang, J.-L. Yao, W.-B. Cai, Exploring Electrosorption at Iron Electrode with in Situ Surface-Enhanced Infrared Absorption Spectroscopy, Anal. Chem. 82 (2010) 5117–5124, https://doi.org/10.1021/ac1002323.
[22] S.M. Abd El Haleem, S. Abd El Wanees, A. Bahgat, Environmental factors affecting the corrosion behaviour of reinforcing steel. VI. Benzotriazole and its derivatives as corrosion inhibitors of steel, Corros. Sci. 87 (2014) 321–333, https://doi.org/10.1016/j.corsci.2014.06.043.
[23] T.G. Heafield, L. Hunter, 76. The associating effect of the hydrogen atom. Part X. The N–H–N bond. The constitution of the benztriazoles, J. Chem. Soc. (1942) 420–422. https://doi.org/10.1039/JR9420000420.
[24] M.M. Davis, Brønsted Acid—Base Behavior in "Inert" Organic Solvents, in: J.J. Lagowski (Ed.), Chem. Nonaqueous Solvents, Elsevier, 1970: pp. 1–135. https://doi.org/10.1016/B978-0-12-433803-6.50007-9.
[25] N.E. White, M. Kilpatrick, Association of N-H Compounds. I. In Benzene., J. Phys. Chem. 59 (1955) 1044–1053. https://doi.org/10.1021/j150532a013.
[26] S. Brunauer, P.H. Emmett, E. Teller, Adsorption of Gases in Multimolecular Layers, J. Am. Chem. Soc. 60 (1938) 309–319, https://doi.org/10.1021/ja01269a023.
[27] A. Ebadi, J.S. Soltan Mohammadzadeh, A. Khudiev, What is the correct form of BET isotherm for modeling liquid phase adsorption?, Adsorption 15 (2009) 65–73, https://doi.org/10.1007/s10450-009-9151-3.
[28] R.M. Cornell, U. Schwertmann, Surface Chemistry and Colloidal Stability, Iron Oxides, Wiley, in, 2003, pp. 221–252.
[29] P. Möller, C.S. Sastri, Estimation of the Number of Surface Layers of Calcite Involved in Ca - 45 Ca Isotopic Exchange with Solution, Zeitschrift Für Phys. Chemie. 89 (1974) 80–87, https://doi.org/10.1524/zpch.1974.89.1-4.080.
[30] H.E. Bergna, Colloid Chemistry of Silica: An Overview, in: Colloid, CRC Press, Silica, 2005, pp. 37–64, https://doi.org/10.1201/9781420028706-7.
[31] J.F. Walsh, H.S. Dhariwal, A. Gutiérrez-Sosa, P. Finetti, C.A. Muryn, N.B. Brookes, R.J. Oldman, G. Thornton, Probing molecular orientation in corrosion inhibition via a NEXAFS study of benzotriazole and related molecules on Cu(100), Surf. Sci. 415 (1998) 423–432, https://doi.org/10.1016/S0039-6028(98)00604-9.
[32] F. Grillo, D.W. Tee, S.M. Francis, H. Früchtl, N.V. Richardson, Initial stages of benzotriazole adsorption on the Cu(111) surface, Nanoscale. 5 (2013) 5269–5273, https://doi.org/10.1039/C3NR00724C.

[33] S. Yang, X. Zhao, Z. Qi, Y.H. Lu, G. Somorjai, P. Yang, A. Baskin, D. Prendergast, M. Salmeron, Chloride-Assisted Corrosion of Copper and Protection by Benzotriazole, ACS Appl. Mater. Interfaces. 14 (2022) 6093–6101, https://doi.org/10.1021/ACSAMI.1C15808/SUPPL_FILE/AM1C15808_SI_001.PDF.
[34] M.T.L. Casford, P.B. Davies, Adsorption of 1- and 2-butylimidazoles at the copper/air and steel/air interfaces studied by sum frequency generation vibrational spectroscopy, Langmuir. 28 (2012) 10741–10748, https://doi.org/10.1021/la301350g.
[35] D.A. Dzombak, F.M.M. Morel, Surface Complexation Modeling: Hydrous Ferric Oxide, Wiley-Interscience, 1990.
[36] I. Popova, J.T. Yates, Adsorption and thermal behavior of benzotriazole chemisorbed on γ-Al2O3, Langmuir. 13 (1997) 6169–6174, https://doi.org/10.1021/la970618v.
[37] Y. Liu, Is the Free Energy Change of Adsorption Correctly Calculated?, J Chem. Eng. Data. 54 (2009) 1981–1985, https://doi.org/10.1021/je800661q.
[38] M.S. Walczak, P. Morales-Gil, R. Lindsay, Determining Gibbs energies of adsorption from corrosion inhibition efficiencies: Is it a reliable approach?, Corros Sci. 155 (2019) 182–185, https://doi.org/10.1016/j.corsci.2019.04.040.
[39] A. Kokalj, Corrosion inhibitors: physisorbed or chemisorbed?, Corros Sci. 196 (2022), https://doi.org/10.1016/J.CORSCI.2021.109939 109939.
[40] C. Gattinoni, P. Tsaousis, C. Euaruksakul, R. Price, D.A. Duncan, T. Pascal, D. Prendergast, G. Held, A. Michaelides, Adsorption Behavior of Organic Molecules: A Study of Benzotriazole on Cu(111) with Spectroscopic and Theoretical Methods, Langmuir. 35 (2019) 882–893, https://doi.org/10.1021/ACS.LANGMUIR.8B03528.